Syntheses, crystal structures, and electrochemical studies of diiron complexes from the reactions of [Et₃NH][(μ-RS) Fe₂(CO)₆(μ-CO)] with isothiocyanates

Ying Shi & Yao-Cheng Shi

Taylor & Francis
Taylor & Francis Group

Syntheses, crystal structures, and electrochemical studies of diiron complexes from the reactions of [Et₃NH][(μ-RS)Fe₂(CO)₆(μ-CO)] with isothiocyanates

YING SHI and YAO-CHENG SHI*

College of Chemistry and Chemical Engineering, Yangzhou University, Yangzhou, PR China
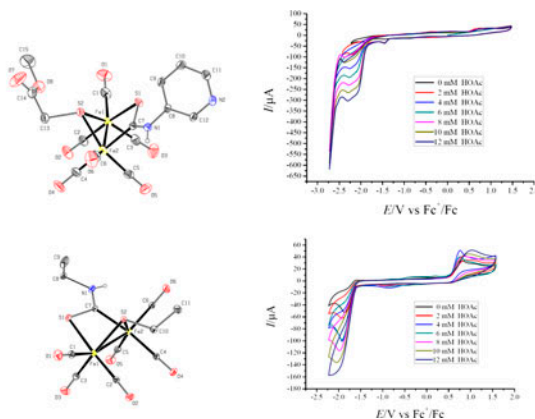
Reactions of [Et₃NH][(μ-MeO₂CCH₂S)Fe₂(CO)₆(μ-CO)] *in situ* generated from the mixture of MeO₂CCH₂SH, Et₃N, and Fe₃(CO)₁₂ with 2-C₅H₄NNCS, 3-C₅H₄NNCS, and EtNCS in THF, form **1**, (μ-MeO₂CCH₂S)Fe₂(CO)₅(μ-k²N,S:k²C-2-C₅H₄NNHCS), **2**, (μ-MeO₂CCH₂S)Fe₂(CO)₆(μ-k²C,S-3-C₅H₄NNHCS), and **3**, (μ-MeO₂CCH₂S)Fe₂(CO)₆(μ-k²C,S-EtNHCS). Reaction of [Et₃NH][(μ-PhS)Fe₂(CO)₆(μ-CO)] *in situ* formed from the mixture of PhSH, Et₃N, and Fe₃(CO)₁₂ with EtNCS affords **4**, (μ-PhS)Fe₂(CO)₆(μ-k²C,S-EtNHCS). Reaction of [Et₃NH][(μ-EtS)Fe₂(CO)₆(μ-CO)] *in situ* produced from the mixture of EtSH, Et₃N, and Fe₃(CO)₁₂ with EtNCS offers **5**, (μ-EtS)Fe₂(CO)₆ (μ-k²C,S-EtNHCS). All new complexes have been fully characterized by EA, IR, ¹H NMR, and ¹³C NMR and structurally determined by X-ray crystallography. Electrochemical studies on **2** and **5** confirm that **2** shows high H₂-producing activity.

Keywords: Hydrogenase; Iron–iron bond; Carbonyl ligand; Thiocarbamoyl group; Cyclic voltammetry

1. Introduction

Hydrogen (H₂) is a clean and renewable fuel. Hydrogenase enzymes very efficiently catalyze the reductive generation and oxidative uptake of molecular hydrogen [1–6]. Enzymes

---

*Corresponding author. Email: ycshi@yzu.edu.cn

typically feature binuclear active sites: either iron and nickel, [FeNi] hydrogenases or two irons, [FeFe] hydrogenases. However, the large size and relative instability of these enzymes under aerobic conditions has led to the search for well-defined molecular catalysts that can produce hydrogen from water in a nonbiological system. Platinum is an excellent catalyst for proton reduction and hydrogen oxidation, but its scarcity and high cost limit widespread use. These considerations have led to the development of molecular catalysts that employ earth-abundant metals [7–12]. Synthetic complexes of nickel, cobalt, iron, and molybdenum have been developed as electrocatalysts for the production of hydrogen [13, 14]. We have recently initiated a project developing synthetic methodologies towards iron–sulfur and iron–selenium cluster complexes as model compounds [15–23]. As part of this on-going project, we report herein the syntheses, crystal structures, and electrochemistry of diiron complexes with thiocarbamoyl groups.

2. Experimental

2.1. *Materials and physical measurements*

All reactions were carried out under N_2 atmosphere with standard Schlenk techniques. All solvents employed were dried by refluxing over appropriate drying agents and stored under N_2 atmosphere. THF was distilled from sodium–benzophenone, petroleum ether (60–90 °C), and CH_2Cl_2 from P_2O_5. Isothiocyanates 2-C_5H_4NNCS and 3-C_5H_4NNCS were prepared according to the literature method [24]. The progress of all reactions was monitored by TLC. ^1H and ^{13}C NMR measurements were carried out on a Bruker Avance 600 or 400 spectrometer. IR spectra were recorded on a Bruker Tensor 27 spectrometer as KBr disks from 400 to 4000 cm^{-1}. Electrochemical measurements were made using a CHI660E potentiostat. Controlled potential coulometry experiments on 1 mM **2** (**5**) in 0.1 M [Bu$_4$N] [PF$_6$]/CH$_3$CN in the presence of 0.1 M HOAc were conducted to confirm the catalytic production of hydrogen. Gas chromatography (GC) analysis of H_2 was conducted with a Shimadzu GC-8A equipped with a thermal conductivity detector. Analyses for C, H, and N were performed on an Elementar Vario EL analyzer. Melting points were measured on an X-6 apparatus.

2.2. *Synthesis of 1*

A 100 mL Schlenk flask equipped with a stir bar and serum cap was charged with 2.015 g (4 mmol) of $Fe_3(CO)_{12}$, 0.425 g (4 mmol) of MeO_2CCH_2SH, 0.56 mL (4 mmol) of Et$_3$N, and 20 mL of THF. The mixture was stirred for 0.5 h at room temperature to form a brown–red solution of [Et$_3$NH][(μ-MeO$_2$CCH$_2$S)Fe$_2$(CO)$_6$(μ-CO)]. To this solution was added 0.545 g (4 mmol) of freshly cracked 2-C_5H_4NNCS monomer in toluene. After stirring for 12 h at room temperature, the solvent was removed under reduced pressure and the resulting residue was chromatographed by TLC on silica gel. Elution with petroleum ether/ethyl acetate (5 : 1, v/v) gave one brown band which was recrystallized from deoxygenated petroleum ether (60–90 °C) and CH_2Cl_2 to afford brown block crystals of **1** (0.356 g) in 18% yield. M.P., 200.2–201.4 °C. Anal. Calcd for $C_{14}H_{10}Fe_2N_2O_7S_2$ (%): C, 34.03; H, 2.04; N, 5.67. Found: C, 34.26; H, 2.15; N, 5.72. IR (KBr disk): 3304 (w), 2816 (vs), 2054 (s), 1989 (vs), 1957 (vs), 1720 (s), 1615 (s), 1485 (w), 1286 (w), 1149 (w), 764 (w), 655 (w) cm^{-1}.

^{1}H NMR (400 MHz, CD$_3$COCD$_3$, TMS): δ 11.454 (s, 1H, NH), 7.015–8.968 (4 m, 4H, C$_5$H$_4$N), 3.636 (s, 3H, CH$_3$), 2.829(s, 2H, CH$_2$). ^{13}C NMR (100 MHz, CD$_3$COCD$_3$, TMS): δ 214.003, 213.719, 213.228, 213.061 (5CO), 169.930 (CO$_2$Me), 160.803 (CS), 153.759, 137.944, 116.984, 111.562 (C$_5$H$_4$N), 51.974 (CH$_3$), 40.778 (CH$_2$).

2.3. Synthesis of 2

A 100 mL Schlenk flask equipped with a stir bar and serum cap was charged with 2.015 g (4 mmol) of Fe$_3$(CO)$_{12}$, 0.425 g (4 mmol) of MeO$_2$CCH$_2$SH, 0.56 mL (4 mmol) of Et$_3$N, and 20 mL of THF. The mixture was stirred for 0.5 h at room temperature to form a brown–red solution of [Et$_3$NH][(μ-MeO$_2$CCH$_2$S)Fe$_2$(CO)$_6$(μ-CO)]. To this solution was added 0.545 g (4 mmol) of 3-C$_5$H$_4$NNCS. After stirring for 12 h at room temperature, the solvent was removed under reduced pressure and the resulting residue was chromatographed by TLC on silica gel. Elution with petroleum ether/ethyl acetate (2 : 1, v/v) gave one orange band which was recrystallized from deoxygenated petroleum ether (60–90 °C) and CH$_2$Cl$_2$ to afford red block crystals of **2** (0.508 g) in 24% yield. M.P., 137–138 °C. Anal. Calcd for C$_{15}$H$_{10}$Fe$_2$N$_2$O$_8$S$_2$ (%): C, 34.51; H, 1.93; N, 5.37. Found: C, 34.39; H, 2.11; N, 5.52. IR (KBr disk): 3089 (w), 2952 (w), 2066 (s), 2024 (vs), 1994 (vs), 1973 (vs), 1734 (m), 1528 (m), 1482 (w), 1377 (w), 1271 (w), 1189 (w), 1121 (w), 1029 (w), 933 (w), 803 (w), 702 (w), 670 (w), 618 (m), 602 (m), 577 (m), 562 (m) cm^{-1}. ^{1}H NMR (400 MHz, CD$_3$COCD$_3$, TMS): 11.163 (s, 1H, NH), 8.516–8.581, 7.832–7.852, 7.447 (d, d, s, 2H, 1H, 1H, C$_5$H$_4$N), 3.805 (s, 3H, CH$_3$), 3.613, 3.579, 3.443, 3.409 (q, AB-type, 2H, CH$_2$). ^{13}C NMR (100 MHz, CD$_3$COCD$_3$, TMS): δ 254.014 (CS), 213.316, 209.801, 207.618 (6CO), 169.561 (CO$_2$Me), 148.589, 145.517, 136.508, 131.659 (C$_5$H$_4$N), 52.016 (CH$_3$), 41.781 (CH$_2$).

2.4. Synthesis of 3

The same procedure as for **2** was used, but EtNCS (0.348 g, 4 mmol) was the added isothiocyanate. Elution with petroleum ether (60–90 °C) and CH$_2$Cl$_2$ (3 : 1, v/v) provided one orange band which was recrystallized from deoxygenated petroleum ether (60–90 °C) and CH$_2$Cl$_2$ to afford red block crystals of **3** (1.102 g) in 58% yield. M.P., 117.0–118.0 °C. Anal. Calcd for C$_{12}$H$_{11}$Fe$_2$NO$_8$S$_2$ (%): C, 30.47; H, 2.34; N, 2.96. Found: C, 30.43; H, 2.31; N, 3.02. IR (KBr disk): 3367 (w), 2979 (w), 2951 (w), 2066 (s), 2023 (vs), 1965 (vs), 1728 (m), 1497 (m), 1442 (w), 1377 (w), 1329 (w), 1272 (m), 1202 (w), 1118 (w), 1010 (w), 930 (w), 835 (w), 618 (m), 575 (m), 490 (w) cm^{-1}. ^{1}H NMR (400 MHz, CDCl$_3$, TMS): δ 7.242 (s, 1H, NH), 3.830 (s, 3H, OCH$_3$), 3.283–3.415 (m, 4H, 2CH$_2$), 1.233 (s, 3H, CH$_3$). ^{1}H NMR (400 MHz, CD$_3$COCD$_3$, TMS): δ 9.460 (s, 1H, NH), 3.785 (s, 3H, OCH$_3$), 3.548, 3.514, 3.368, 3.334 (q, AB-type, 2H, CH$_2$), 3.440–3.489 (m, 2H, CH$_2$), 1.173 (t, 3H, ^3J = 7.2 Hz, CH$_3$). ^{13}C NMR (100 MHz, DCCl$_3$, TMS): δ 247.072 (CS), 212.957, 209.074, 208.234 (6CO), 169.714 (CO$_2$Me), 52.613 (OCH$_3$), 44.030 (NCH$_2$), 41.704 (SCH$_2$), 13.341 (CH$_3$).

2.5. Synthesis of 4

A 100 mL Schlenk flask equipped with a stir bar and serum cap was charged with 2.015 g (4 mmol) of Fe$_3$(CO)$_{12}$, 0.441 g (4 mmol) of PhSH, 0.56 mL (4 mmol) of Et$_3$N, and 20 mL

of THF. The mixture was stirred for 0.5 h at room temperature to form a brown–red solution of [Et$_3$NH][(μ-PhS)Fe$_2$(CO)$_6$(μ-CO)]. To this solution was added 0.348 g (4 mmol) of EtNCS. After stirring for 12 h at room temperature, the solvent was removed *in vacuo* and the resulting residue was chromatographed by TLC on silica gel. Elution with petroleum ether offered an orange–red band which was recrystallized from deoxygenated petroleum ether (60–90 °C) and CH$_2$Cl$_2$ to provide red crystals of **4** (1.409 g) in 74% yield. Mp., 76.0–77.0 °C. Anal. Calcd for C$_{15}$H$_{11}$Fe$_2$NO$_6$S$_2$ (%): C, 37.76; H, 2.32; N, 2.94. Found: C, 37.86; H, 2.45; N, 2.97. IR (KBr disk): 3390 (w), 2068 (s), 2028 (vs), 1988 (s, br), 1579 (m), 1387 (w), 1327 (w), 1149 (w), 1027 (w), 744 (m), 694 (m) cm^{-1}. ^{1}H NMR (600 MHz, CDCl$_3$, TMS): δ 7.456–7.473, 7.167–7.237 (d, m, 2H, 3H, C$_6$H$_5$), 7.289 (s, 1H, NH), 3.393–3.526 (m, 2H, CH$_2$), 1.233 (t, 3H, ^3J = 7.2 Hz, CH$_3$). ^{13}C NMR (150 MHz, CDCl$_3$): δ 247.281 (C=S), 212.972, 208.504, 208.132 (6CO), 142.222, 131.445, 128.080, 126.903 (C$_6$H$_5$), 43.747 (CH$_2$), 12.996 (CH$_3$).

2.6. *Synthesis of 5*

The same procedure as for **4** was used, but EtSH (0.249 g, 4 mmol) was the added thiol. Elution with petroleum ether (60–90 °C) and CH$_2$Cl$_2$ (5 : 1, v/v) afforded an orange solid of **5** (0.925 g) in 54% yield. Mp., 104.2–105.5 °C. Anal. Calcd for C$_{11}$H$_{11}$Fe$_2$NO$_6$S$_2$ (%): C, 30.79; H, 2.58; N, 3.26. Found: C, 30.81; H, 2.69; N, 3.18. IR (KBr disk): 3382 (s), 2962 (w), 2928 (w), 2868 (w), 2062 (vs), 2018 (vs), 1922 (vs), 1505 (s), 1448 (s), 1387 (w), 1258 (w), 1091 (w), 1027 (w) cm^{-1}. ^{1}H NMR (400 MHz, CDCl$_3$, TMS): δ 7.164 (s, 1H, NH), 3.396–3.470 (m, 2H, CH$_2$), 2.613–2.651 (m, 2H, CH$_2$), 1.506 (t, 3H, ^3J = 7.2 Hz, CH$_3$), 1.228 (t, 3H, ^3J = 7.2 Hz, CH$_3$). ^{13}C NMR (100 MHz, CDCl$_3$, TMS): δ 247.996 (C=S), 213.209, 209.440, 209.122 (6CO), 43.875 (NCH$_2$), 35.398 (SCH$_2$), 18.538 (CH$_3$), 13.373 (CH$_3$).

2.7. *X-ray structure determinations of complexes*

Single crystals of **1**–**5** suitable for X-ray diffraction analyses were grown by slow evaporation of the CH$_2$Cl$_2$–petroleum ether solutions of **1**–**5** at 0–4 °C. For each complex, a selected single crystal was mounted on a Bruker D8quest CCD diffractometer using graphite-monochromated Mo-Kα radiation (λ = 0.71073 Å) at 296 K. The structures of **1**–**5** were solved by direct methods using SIR-2011 software and refined by full-matrix least-squares based on F^2 with anisotropic thermal parameters for all nonhydrogen atoms using the SHELXTL program package [25, 26]. For **3**, O7 is disordered over two positions (52/48). For **5**, the ethyl group attached to N1 is disordered over two positions (56/44). All C-bound H atoms were placed at geometrically idealized positions and subsequently treated as riding, with C–H = 0.93 (aromatic), 0.97 (CH$_2$), and 0.96 (CH$_3$) Å and U_{iso}(H) values of 1.2U_{eq}(C) or 1.5U_{eq}(C$_{methyl}$). All N-bound H atoms were located in difference Fourier maps and freely refined isotropically. PLATON views of the complexes are drawn using the PLATON software [27]. Crystal data, selected bond lengths and angles (Å, °), and hydrogen bond parameters (Å, °) for **1**–**5** are summarized in tables 1–3.

2.8. *Electrochemistry of 2 and 5*

Cyclic voltammetry experiments were carried out in a *ca.* 5 mL one-compartment glass cell. The working electrode was a glassy carbon disk (0.3 cm in diameter), the reference

electrode was a saturated calomel electrode, and the counter electrode was a Pt wire. The electrolyte was 0.1 M $^nBu_4NPF_6$ in MeCN. The electrolyte solution was degassed by bubbling with N_2 for at least 10 min before measurement. The typical concentration of the organometallic complex was 1 mM. The acid concentration in the electrolyte was varied by addition of measured volumes of a solution of HOAc in MeCN or CH_2Cl_2.

3. Results and discussion

3.1. *Syntheses of complexes*

Reactions of $Fe_3(CO)_{12}$ with thiols in the presence of Et_3N afford cluster salts $[Et_3NH][(\mu-RS)Fe_2(CO)_6(\mu-CO)]$. On the basis of our work, Song's work and Seyferth's work, we have investigated the reactions of the cluster salts with isothiocyanates (scheme 1) [15, 18, 28–31]. The reaction of MeO_2CCH_2SH, Et_3N, and $Fe_3(CO)_{12}$ in THF, via $[Et_3NH][(\mu-MeO_2CCH_2S)Fe_2(CO)_6(\mu-CO)]$, with $2-C_5H_4NNCS$ forms **1**, $(\mu-MeO_2CCH_2S)Fe_2(CO)_5(\mu-k^2N,S:k^2C-2-C_5H_4NNHCS)$. However, the reaction with $3-C_5H_4NNCS$ gives **2**, $(\mu-MeO_2CCH_2S)Fe_2(CO)_6(\mu-k^2C,S-3-C_5H_4NNHCS)$ in which the pyridine N is pendant. Similarly, the reaction with EtNCS provides **3**, $(\mu-MeO_2CCH_2S)Fe_2(CO)_6(\mu-k^2C,S-EtNHCS)$. The reaction of PhSH, Et_3N, and $Fe_3(CO)_{12}$ in THF, via $[Et_3NH][(\mu-PhS)Fe_2(CO)_6(\mu-CO)]$, with EtNCS affords **4**, $(\mu-PhS)Fe_2(CO)_6(\mu-k^2C,S-EtNHCS)$. Analogously, the reaction of $[Et_3NH][(\mu-EtS)Fe_2(CO)_6(\mu-CO)]$ with EtNCS generates **5**, $(\mu-EtS)Fe_2(CO)_6(\mu-k^2C,S-EtNHCS)$.
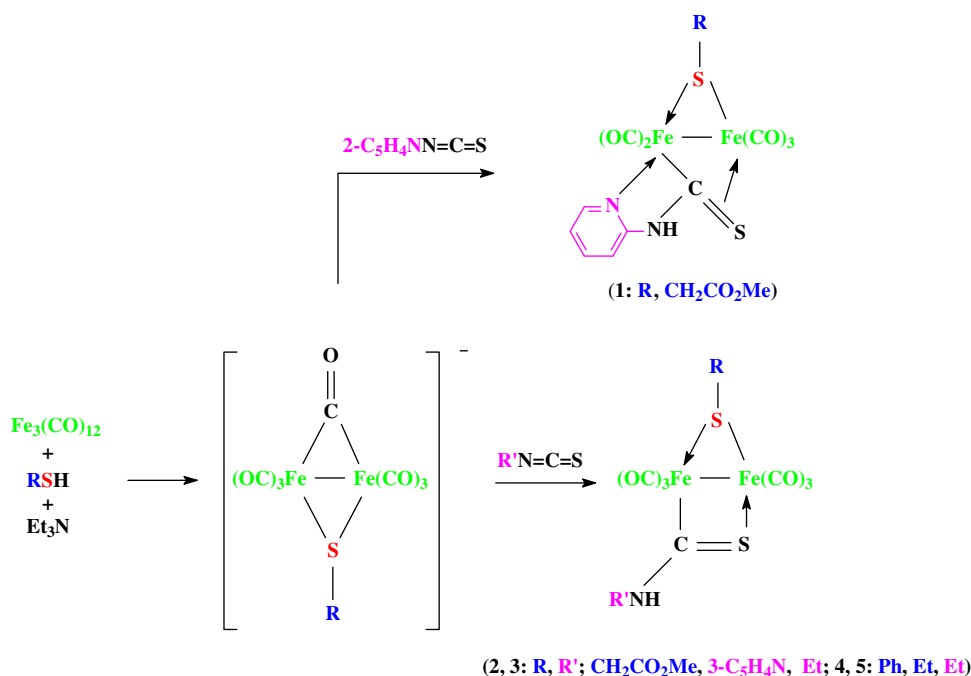
Scheme 1. Syntheses of **1**, **2**, **3**, **4**, and **5**.

3.2. X-ray structures of complexes

Structures of **1–5** have been determined by X-ray crystallography (table 1). Complex **1** crystallizes in the $P2_1/n$ space group. As shown in figure 1, **1** is an $Fe_2(CO)_5$ complex with three terminal carbonyl ligands on Fe1 and two on Fe2 and contains the bridging, three-electron MeO_2CCH_2S, and five-electron $2\text{-}C_5H_4NNHCS$ ligands. The C6···S2–C12 angle of 94.08(10)° reveals that the C12–S2 bond is at an axial position, viz. **1** is an a-type isomer resulting from one of two axial (a) and equatorial (e) orientations of the organic group on sulfur with respect to the Fe2S plane [15]. The Fe1–Fe2 bond of 2.5938(6) Å is slightly shorter than those of **2** and **3** (table 2). The Fe2–N2 bond length is 1.975(2) Å. Interestingly, the Fe1–C6, Fe2–C6, Fe1–S1, and S1–C6 bond lengths of 2.223(3), 1.933(3), 2.3388 (9), and 1.709(3) Å indicate that the C6S1 thioacyl group as a three-electron donor is attached to Fe2 and Fe1 in a σ, π-bonded manner ($\mu\text{-}k^2C,kS$). However, the thioacyl groups in reported complexes such as $(\mu\text{-MeS})Fe_2(CO)_6(\mu_4\text{-S})Fe_2(CO)_6(\mu\text{-PhNHC=S})$ [C=S, 1.698 (5) Å] and $(\mu\text{-}p\text{-MeC}_6H_4Se)Fe_2(CO)_6(\mu\text{-PhCH}_2NHC=S)$ [C=S, 1.691(4) Å] are in σ,

Table 1. Crystal data, data collections, and structure refinements for **1–5**.

|	1	2	3	4	5
Formula	$C_{14}H_{10}Fe_2N_2O_7S_2$	$C_{15}H_{10}Fe_2N_2O_8S_2$	$C_{12}H_{11}Fe_2NO_8S_2$	$C_{15}H_{11}Fe_2NO_6S_2$	$C_{11}H_{11}Fe_2NO_6S_2$
Fw	494.06	522.07	473.04	477.07	429.03
Crystal system	Monoclinic	Monoclinic	Monoclinic	Monoclinic	Triclinic
Space group	$P2_1/n$	$C2/c$	$C2/c$	$P2_1/c$	$P\bar{1}$
a (Å)	9.2994(11)	19.637(2)	18.551(2)	16.697(2)	7.9359(14)
b (Å)	16.7587(19)	8.2869(11)	7.8985(3)	13.2698(16)	9.6032(15)
c (Å)	11.8144(14)	27.0812(17)	26.384(3)	17.664(2)	11.5761(12)
α (°)	90.00	90.00	90.00	90.00	81.361(2)
β (°)	90.568(3)	106.675(4)	110.511(6)	90.456(3)	88.287(3)
γ (°)	90.00	90.00	90.00	90.00	76.313(3)
V (Å^3)	1841.1(4)	4221.6(8)	3620.8(6)	3913.6(8)	847.4(2)
Z	4	8	8	8	2
D_c (g cm^{-3})	1.782	1.643	1.735	1.619	1.681
μ (mm^{-1})	1.842	1.615	1.871	1.725	1.981
$F(0\,0\,0)$	992	2096	1904	1920	432
Index ranges	$-12 \le h \le 12$	$-25 \le h \le 25$	$-24 \le h \le 21$	$-21 \le h \le 21$	$-10 \le h \le 10$
	$-17 \le k \le 21$	$-10 \le k \le 8$	$-10 \le k \le 9$	$-17 \le k \le 14$	$-12 \le k \le 12$
	$-15 \le l \le 12$	$-28 \le l \le 35$	$-33 \le l \le 34$	$-22 \le l \le 22$	$-15 \le l \le 14$
Reflections measured	18,397	10,132	17,263	54,641	20,128
Unique reflections	4222	4667	4117	9014	3835
Reflections $[I > 2\sigma(I)]$	3199	3593	3474	5357	3273
R_{int}	0.034	0.024	0.041	0.078	0.051
θ Range (°)	2.4–27.5	2.7–27.5	2.3–27.5	1.9–27.6	1.8–27.6
Data/restraints/parameters	4222/0/248	4667/0/267	4117/0/242	9014/1/477	3835/2/225
R_1	0.0375	0.0357	0.0347	0.0532	0.0322
wR_2	0.0841	0.0781	0.0835	0.1214	0.0882
GoF	1.06	1.02	1.05	1.01	1.04
Largest diff. peak and hole (e Å^{-3})	0.53/−0.27	0.38/−0.30	0.55/−0.51	0.66/−0.50	0.57/−0.35
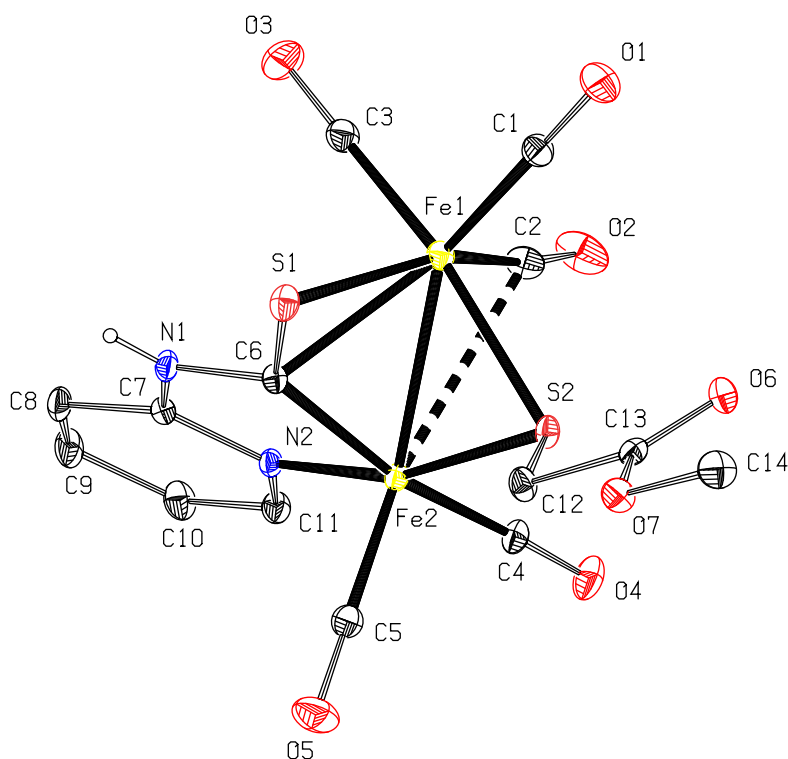
Figure 1.   The molecule of **1**. Displacement ellipsoids are drawn at 20% probability. The dashed line indicates the weak intramolecular interaction.

n-modes (μ-k^{2}C,S) [32, 33]. So far, several coordination fashions of a thiocarbamoyl ligand have been reported in the literature: kC (Me$_2$NCS), k^{2}C,S (Me$_2$NCS), μ-k^{2}C,S (Me$_2$NCS), and μ-kC,k^{2}S (Me$_2$NCS) [34–36]. Thus, a new bonding mode of a thiocarbamoyl ligand has been discovered by us. The Fe2–C6 bond is markedly shorter than those of Fe–C single bonds of **2–5**, displaying that the Fe2–C6 bond has some double-bond character [19]. S2 spans the two Fe ions asymmetrically, with 2.2868(8) and 2.2268(8) Å bond lengths of Fe1–S2 and Fe2–S2. The five-membered chelating ring Fe2C6N1C7N2 is planar and makes two dihedral angles of 8.6(2)° and 59.49(12)° with three-membered rings Fe2C6S1 and Fe1Fe2C6. The Fe1–S2–Fe2 and Fe1–C6–Fe2 bond angles are 70.14(2)° and 76.89(9)°; the dihedral angle between the two planes is 58.29(10)°.

Among the five carbonyl ligands, the axial C5O5 shows the shortest Fe–C bond of 1.750(3) Å, close to 1.747(4) Å of (η^4-PhCH=CHCH=N(C$_6$H$_{11}$))Fe(CO)$_2$P(OMe)$_3$ [37]. One of the three carbonyl ligands attached to Fe1, viz. C2O2, participates in an intramolecular interaction with Fe2 from a direction *trans* to the C5O5 ligand with a C2···Fe2–C5 angle of 166.38(12)° [17, 21]. The C2···Fe2 distance is 2.763(4) Å, which lies between the sum of the covalent radii (*r*) and van der Waals radii (*R*) for Fe and C [*r*(Fe) + *r*(C) = 2.13 Å; *R*(Fe) + *R*(C) = 3.84 Å] [27]. In accord with this interaction is a significant deviation of the Fe1–C2–O2 bond angle of 171.8(3)° from linearity, with carbonyl C2 bent towards Fe2; the other Fe–C–O bond angles lie in the range of 176.8(3)°–179.8(4)°. In addition, the S1···S2 and C6···S2 distances of 3.3057(10) and 3.029(3) Å prove the

Table 2. Selected bond lengths and angles (Å, °) for **1**–**5**.

| **1**		**2**		**3**		**4a**		**4b**		**5**	
Fe1–Fe2	2.5938(6)	Fe1–Fe2	2.6148(5)	Fe1–Fe2	2.6142(5)	Fe1–Fe2	2.6130(8)	Fe3–Fe4	2.5981(9)	Fe1–Fe2	2.6132(5)
Fe1–S1	2.3388(9)	Fe1–S1	2.3156(6)	Fe1–S1	2.3122(6)	Fe1–S1	2.3174(12)	Fe3–S3	2.3123(13)	Fe1–S1	2.3165(6)
Fe1–S2	2.2868(8)	Fe1–S2	2.2301(7)	Fe1–S2	2.2369(6)	Fe1–S2	2.2398(12)	Fe3–S4	2.2425(13)	Fe1–S2	2.2317(6)
Fe2–S2	2.2268(8)	Fe2–S2	2.2582(8)	Fe2–S2	2.2425(6)	Fe2–S2	2.2556(12)	Fe4–S4	2.2707(12)	Fe2–S2	2.2507(6)
Fe1–C6	2.223(3)	Fe2–C7	1.964(2)	Fe2–C7	1.969(2)	Fe2–C7	1.965(4)	Fe4–C22	1.964(4)	Fe2–C7	1.976(2)
Fe2–C6	1.933(3)	C7–S1	1.703(2)	C7–S1	1.693(2)	C7–S1	1.699(4)	C22–S3	1.704(5)	C7–S1	1.698(2)
Fe2–N2	1.975(2)	C7–N1	1.325(3)	C7–N1	1.315(3)	C7–N1	1.309(5)	C22–N2	1.307(5)	C7–N1	1.306(3)
S1–C6	1.709(3)	C8–N1	1.424(3)	C8–N1	1.465(3)	C8–N1	1.465(5)	C23–N2	1.433(6)	C8–N1	1.517(14)
S2–C12	1.813(3)									C8B–N1	1.45(2)
N1–C6	1.377(3)										
N1–C7	1.358(3)										
Fe1–S2–Fe2	70.14(2)	Fe1–S2–Fe2	71.26(2)	Fe1–S2–Fe2	71.41(2)	Fe1–S2–Fe2	71.08(4)	Fe3–S4–Fe4	70.29(4)	Fe1–S2–Fe2	71.32(2)
Fe1–C6–Fe2	76.89(9)	C7–N1–C8	126.7(2)	C7–N1–C8	125.2(2)	C7–N1–C8	126.6(4)	C22–N2–C23	127.8(5)	C7–N1–C8	120.8(3)
C6–N1–C7	118.4(2)	N1–C7–S1	121.10(18)	N1–C7–S1	119.32(17)	N1–C7–S1	120.0(3)	N2–C22–S3	119.5(3)	N1–C7–S1	120.57(15)
N1–C6–S1	117.5(2)	N1–C7–Fe2	124.83(17)	N1–C7–Fe2	127.76(17)	N1–C7–Fe2	127.2(3)	N2–C22–Fe4	127.6(4)	N1–C7–Fe2	126.49(16)
N1–C6–Fe2	111.86(18)	S1–C7–Fe2	114.06(12)	S1–C7–Fe2	112.84(12)	S1–C7–Fe2	112.8(2)	S3–C22–Fe4	113.0(2)	S1–C7–Fe2	112.88(11)
S1–C6–Fe2	130.54(15)										
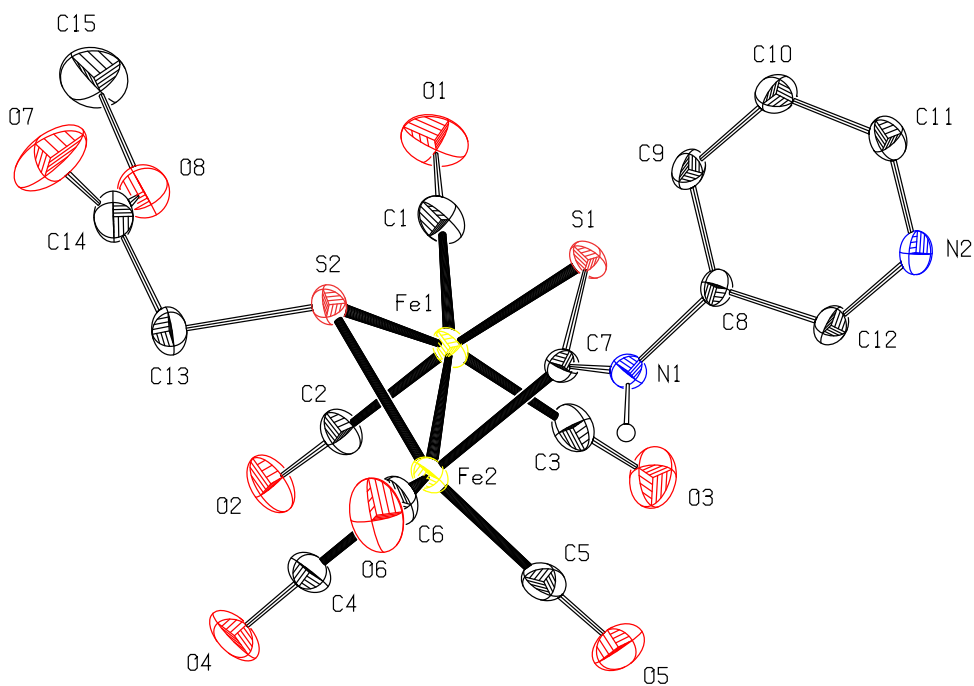
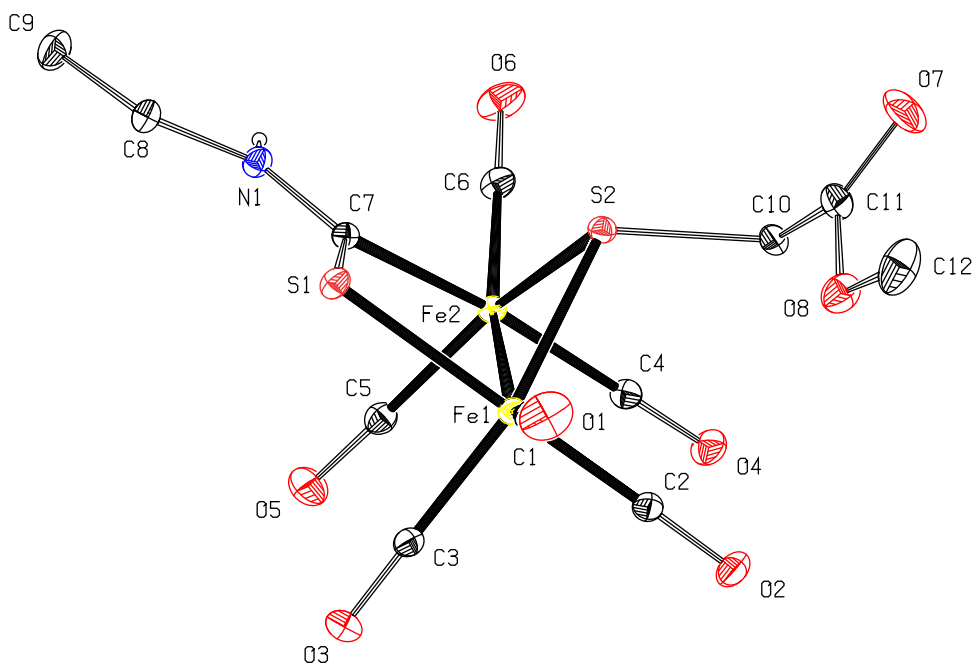Figure 2. The molecule of **2**. Displacement ellipsoids are drawn at 20% probability.

Figure 3. The molecule of **3**. Displacement ellipsoids are drawn at 20% probability.
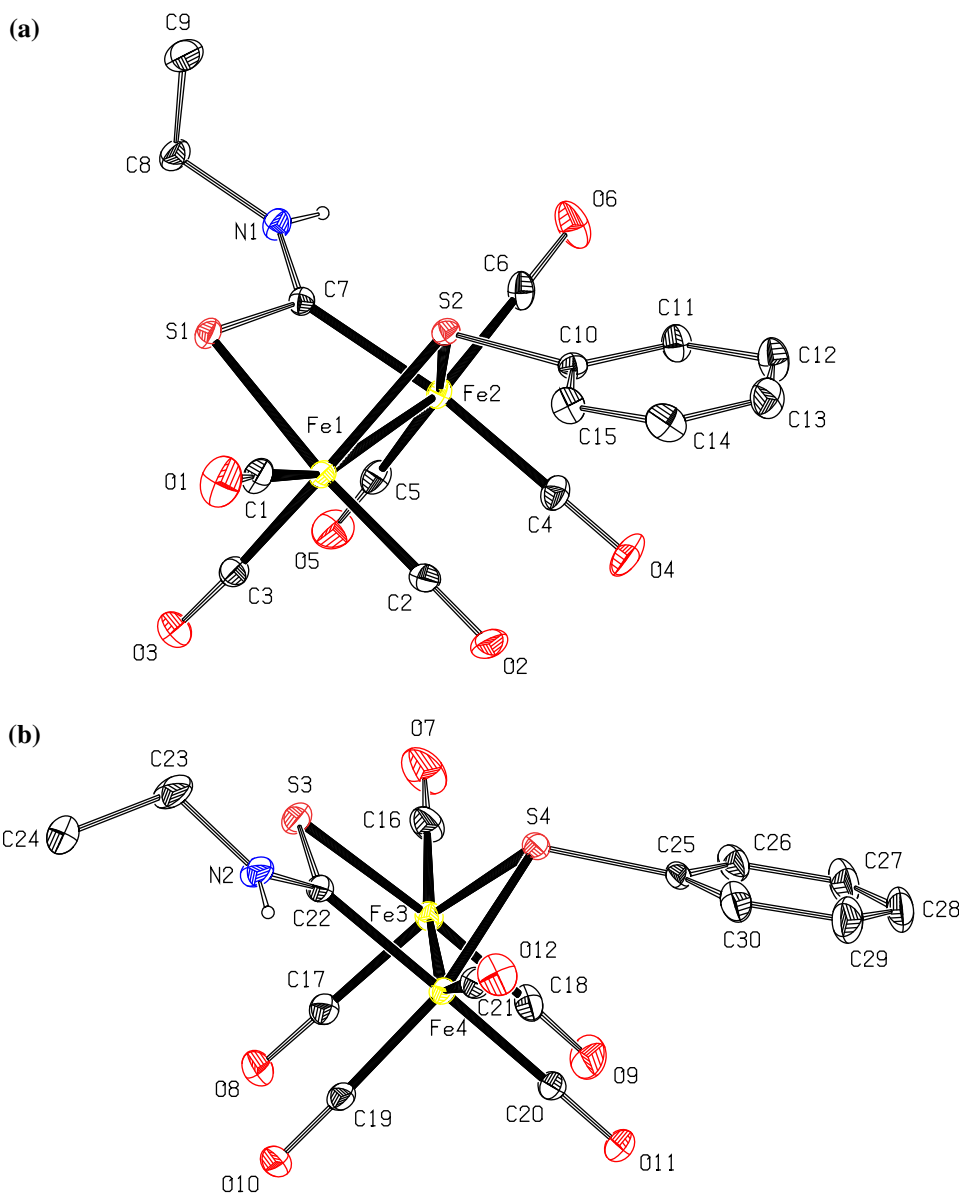
Figure 4. The two different molecules of **4**, labeled (**4**a) and (**4**b) (top, **4**a; bottom, **4**b). Displacement ellipsoids are drawn at 20% probability.

existence of intramolecular contacts between S2 and the CS group in **1** $[R(S) + R(S) =$ 3.60 Å; $R(S) + R(C) = 3.50$ Å] [27].

Complex **2** crystallizes in the *C2/c* space group (figure 2). The iron centers are in distorted octahedral environments, satisfying the 18-e rule. Two tricarbonyl groups on Fe1 and Fe2 are eclipsed and all CO ligands are terminal. The iron–iron distance of 2.6148(5) Å is almost equal to that of **3**. S2 slightly asymmetrically links the $Fe_2(CO)_6$ unit with 2.2301(7)

and 2.2582(8) Å bond lengths of Fe1–S2 and Fe2–S2 bonds. The four-membered ring of Fe1Fe2C7S1 is not planar, S1 being 0.1619(6) Å away from the Fe1Fe2C7 plane. The Fe1–S2–Fe2 bond angle is 71.26(2)°. The C13–S2⋯S1 and C13–S2⋯C7 angles of 164.18 (10)° and 155.32(11)° display that the C13–S2 bond is at an equatorial position, viz. **2** is an e-type isomer [15]. The angles about C7 and N1 are 359.99(15)° and 359.6(2)°, indicating that these two atoms each adopt sp^2-hybridization. The C7S1 and C7N1 bonds of 1.703(2) and 1.325(3) Å suggest that the presence of $p–\pi$ conjugation in the S=C–N group, the Fe2C7 and C8N1 bonds of 1.964(2) and 1.424(3) Å being single bonds. Like **3**, the S1⋯S2 and C7⋯S2 distances of 2.9486(9) and 2.836(3) Å prove the existence of intramolecular contacts between the thiolato S and the CS group in **2**.

Complex **3** crystallizes in the *C2/c* space group (figure 3). The iron centers are in distorted octahedral environments, obeying the 18-e rule. Two tricarbonyl groups on Fe1 and Fe2 are eclipsed and all CO ligands are terminal. The iron–iron distance of 2.6142(5) Å is almost equal to that of **2**. S2 slightly asymmetrically links the $Fe_2(CO)_6$ unit with 2.2369(6) and 2.2425(6) Å bond lengths of Fe1–S2 and Fe2–S2 bonds. Unlike **2**, the four-membered ring of Fe1Fe2C7S1 is planar, S1 being 0.0327(6) Å away from the Fe1Fe2C7 plane. The Fe1–S2–Fe2 bond angle is 71.41(2)°. The C10–S2⋯S1 and C10–S2⋯C7 angles of 163.58 (8)° and 155.26(10)° display that the C10–S2 bond is at an equatorial position, namely **3** is an e-type isomer. The angles about C7 and N1 are 359.92(15)° and 359.9(2)°, indicating that these two atoms each adopt sp^2-hybridization. The C7S1 and C7N1 bonds of 1.693(2) and 1.315(3) Å suggest the presence of $p–\pi$ conjugation in the S=C–N group; the Fe2C7 and C8N1 bonds of 1.969(2) and 1.465(3) Å are single bonds. As described below, the S1⋯S2 and C7⋯S2 distances of 2.9947(9) and 2.824(2) Å prove the existence of intramolecular contacts between the thiolato S and the CS group in **3**.

Complex **4** crystallizes in the *P2₁/c* space group, with two independent molecules in the asymmetric unit, labeled **4**a and **4**b as shown in figure 4. The iron centers are in distorted
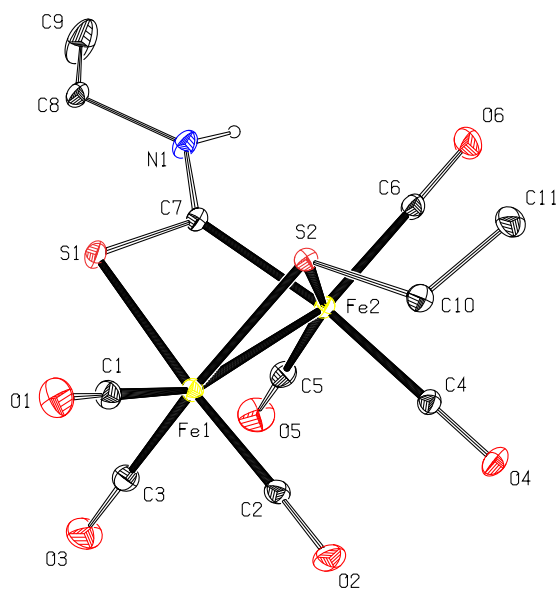

Figure 5.   The molecule of **5**. Displacement ellipsoids are drawn at 20% probability.

Table 3. Hydrogen bond parameters (Å, °) for **1–5**.

		D–H	H$\cdots A$	$D\cdots A$	D–H$\cdots A$
1	C14–H14C$\cdots$O6^i	0.96	2.47	3.364(4)	155
	N1–H1N$\cdots$O6^{ii}	0.74(3)	2.35(3)	3.050(3)	159(3)
2	N1–H1N$\cdots$N2^i	0.83(3)	2.06(3)	2.855(3)	162(3)
	C12–H12$\cdots$O7^{ii}	0.93	2.59	3.278(4)	131
3	C10–H10B$\cdots$O6^i	0.97	2.69	3.367(3)	128
	C8–H8B$\cdots$O6^{ii}	0.97	2.63	3.199(3)	118
4	C13–H13$\cdots$O7^i	0.93	2.56	3.334(7)	141
	N1–H1N$\cdots$S4^{ii}	0.80(5)	2.82(5)	3.552(4)	154(4)
5	N1–H1N$\cdots$O5^i	0.81(3)	2.54(3)	3.272(3)	152(2)
	C10–H10A$\cdots$O1^{ii}	0.97	2.59	3.476(3)	152

Symmetry codes: (i) $-x$, $1 - y$, $1 - z$; (ii) $1 + x$, y, z for **1**; (i) $1/2 - x$, $1/2 + y$, $3/2 - z$; (ii) $-1/2 + x$, $-1/2 + y$, z for **2**; (i) $1 - x$, y, $1/2 - z$; (ii) x, $1 + y$, z for **3**; (i) $1 - x$, $1 - y$, $1 - z$; (ii) x, $-1 + y$, z for **4**; (i) $1 - x$, $1 - y$, $1 - z$; (ii) $-x$, $2 - y$, $2 - z$ for **5**.
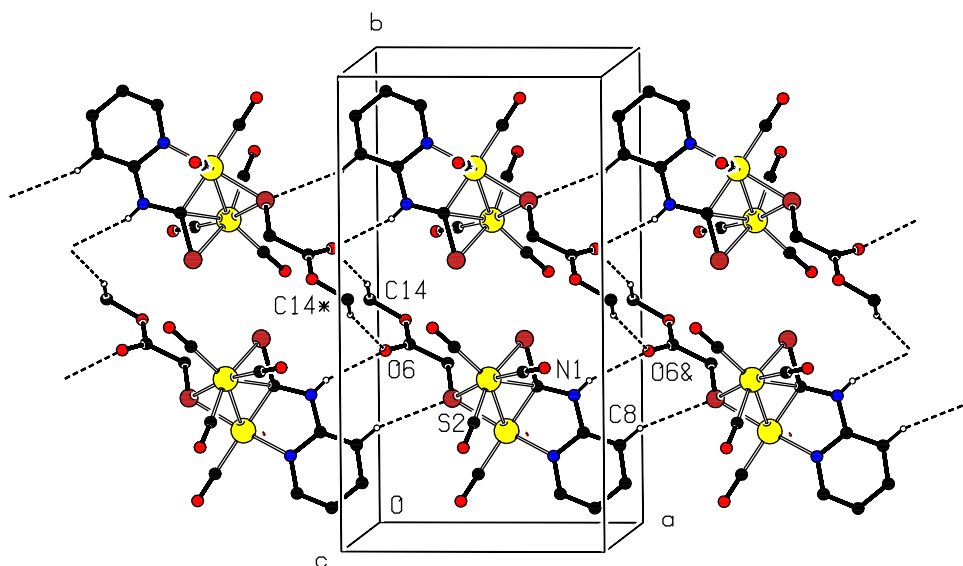

Figure 6. Part of the crystal structure of **1** showing the formation of the dimers generated by C–H$\cdots$O hydrogen bonds and the formation of the [1 0 0] double chain linked by N–H$\cdots$O hydrogen bonds (dashed lines). For clarity, hydrogens not involved in the motif shown have been omitted. Atoms labeled with an asterisk (*) or an ampersand (&) sign are at the symmetry positions $(-x, 1 - y, 1 - z)$ and $(1 + x, y, z)$, respectively.

octahedral environments, satisfying the 18-e rule. Two tricarbonyl groups of each $Fe_2(CO)_6$ unit, viewed along the Fe–Fe bond, are eclipsed, and all CO ligands are terminal. For **4a**, the Fe–Fe single bond length is 2.6130(8) Å. S2 asymmetrically bridges the $Fe_2(CO)_6$ unit with Fe1–S2 and Fe2–S2 lengths of 2.2398(12) and 2.2556(12) Å. Three Fe2–C7, S1–C7, and N1–C7 bond lengths about C7 are 1.965(4), 1.699(4), and 1.309(5) Å, respectively. In addition, the Fe1–S1 and N1–C8 bond lengths are 2.3174(12) and 1.465(4) Å. For **4b**, the corresponding values are 2.5981(9), 2.2425(13), 2.2707(12), 1.964(4), 1.704(5), 1.307(5), 2.3123(13), and 1.433(6) Å. The angles about C7 and C22 are 360.0(3)° and 360.1(3)° and the angles about N1 and N2 are 360(3)° and 360(3)°, indicating that these atoms are

sp^2-hybridized. These facts support the presence of p–π conjugation in the S=C–N group. The bond angles of Fe1–S2–Fe2 and Fe3–S4–Fe4 are 71.08(4)° and 70.29(4)°. The angles of C10–S2···S1, C10–S2···C7, C25–S4···S3, and C25–S4···C22 of 162.88(13)°, 157.15 (14)°, 166.21(16)°, and 152.7(2)° indicate that the C10–S2 and C25–S4 bonds are equatorial, viz. **4** is an e-type isomer. S1 is 0.0294(11) Å away from the Fe1Fe2C7 plane, indicating that the four-membered ring in **4a** is planar. However, the distance of S3 to the Fe3Fe4C22 plane is 0.1117(13) Å, demonstrating that the four-membered ring in **4b** is puckered. The S1···S2, C7···S2, S3···S4, and C22···S4 distances of 2.9885(15), 2.821(4), 2.9939(17), and 2.868(5) Å confirm intramolecular contacts between the thiolato S and the CS group exist in **4**.

Complex **5** crystallizes in the $P\bar{1}$ space group (figure 5). As in **4**, the iron centers are in distorted octahedral environments. Two tricarbonyl groups on Fe1 and Fe2 are eclipsed and all CO ligands are terminal. The iron–iron distance of 2.6132(5) Å is almost equal to that of **4a**. S2 slightly asymmetrically links the Fe$_2$(CO)$_6$ unit with 2.2317(6) and 2.2507(6) Å bond lengths of Fe1–S2 and Fe2–S2 bonds. The four-membered ring of Fe1Fe2C7S1 is planar with S1 being 0.0196(7) Å away from the Fe1Fe2C7 plane. The Fe1–S2–Fe2 bond of 71.32(2)° with four-membered ring forms a dihedral angle of 89.10(4)°. The C10–S2···S1 and C10–S2···C7 angles of 164.03(8)° and 154.93(9)° indicate that the C10–S2 bond is equatorial, with **5** as an e-type isomer. The angles about C7 and N1 are 359.94(14)° and 360.7(3)°, indicating that these atoms have sp^2-hybridization. The C7S1 and C7N1 bonds of 1.698(2) and 1.306(3) Å suggest the presence of p–π conjugation in the S=C–N group; the Fe2C7 and C8N1 (C8BN1) bonds of 1.976(2) and 1.517(14) (1.45(2)) Å are single bonds (the Et bonded to N1 is disordered over two positions). Like **2**–**4**, the S1···S2 and C7···S2 distances of 3.0110(9) and 2.834(2) Å prove the existence of intramolecular contacts between the thiolato S and the CS group in **5** [$R(S) + R(S) = 3.60$ Å; $R(S) + R(C) = 3.50$ Å] [27].
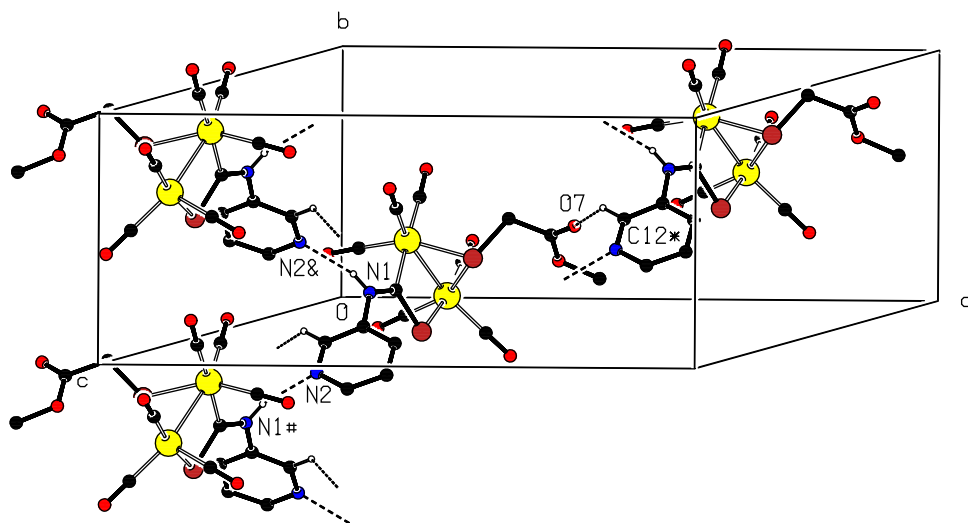

Figure 7. Part of the crystal structure of **2** showing the formation of the [0 1 0] chain generated by N–H···N hydrogen bonds and the formation of the (1 1 0) sheet linked by C–H···O hydrogen bonds (dashed lines). For clarity, hydrogens not involved in the motif shown have been omitted. Atoms labeled with an asterisk (*) or an ampersand (&) or a hash (#) sign are at the symmetry positions ($1/2 + x$, $1/2 + y$, z), ($1/2 - x$, $1/2 + y$, $3/2 - z$), and ($1/2 - x$, $-1/2 + y$, $3/2 - z$), respectively.

Finally, it is interesting to discuss packing interactions in the above complexes (table 3). In **1**, molecules generate dimers via the C14–H14C···O6^i hydrogen bond [symmetry code: (i) $-x$, $1-y$, $1-z$]. The dimers (figure 6) are linked into [1 0 0] chains by N1–H1N···O6^{ii} hydrogen bonds [symmetry code: (ii) $1+x$, y, z]. Molecules of **2** (figure 7) are linked into [0 1 0] chains by N1–H1N···N2^i hydrogen bonds [symmetry code: (i) $1/2-x$, $1/2+y$, $3/2-z$]. The chains are packed by the C12–H12···O7^{ii} hydrogen bonds to form *C* sheets [symmetry code: (ii) $-1/2+x$, $-1/2+y$, z]. Unlike **2**, very weak hydrogen bonds are observed in **3**, the NH group does not take part in hydrogen bonding. Molecules of **3** form dimers via the C10–H10B···O6^i hydrogen bond [symmetry code: (i) $1-x$, y, $1/2-z$].
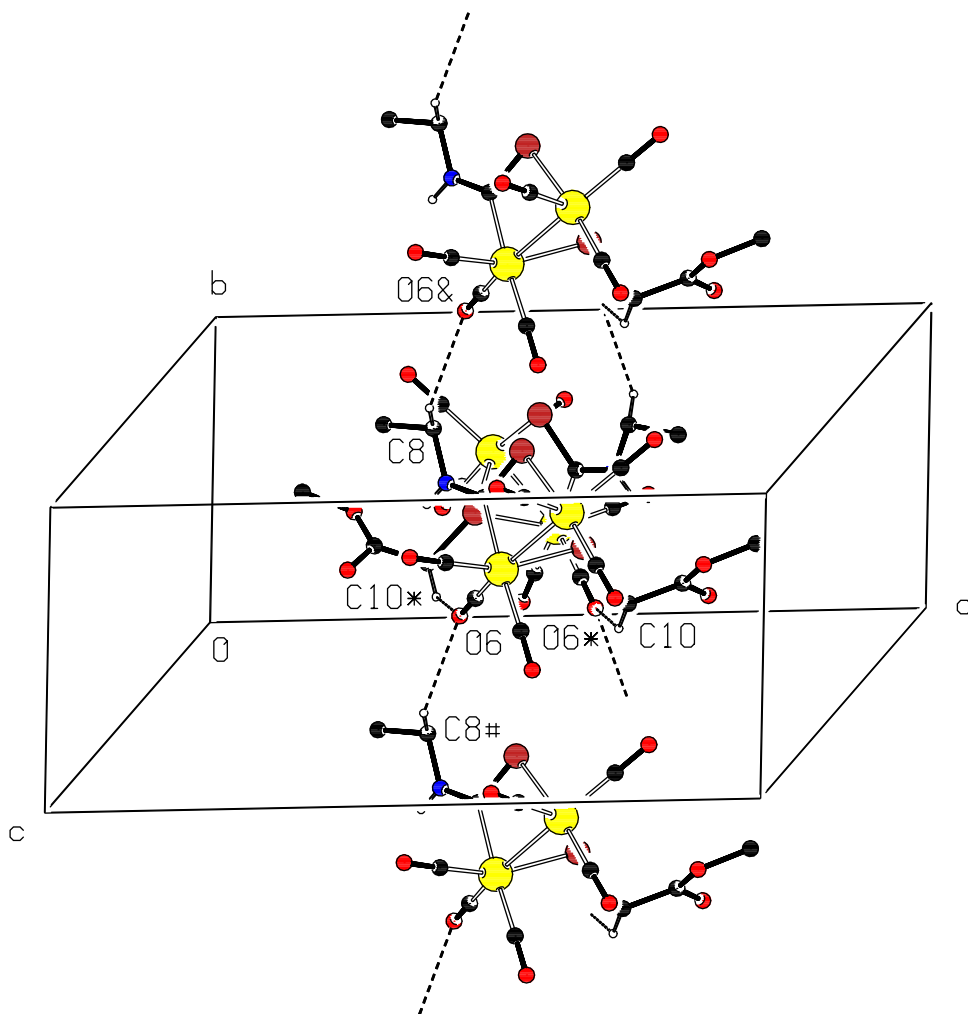

Figure 8.   Part of the crystal structure of **3** showing the formation of the C$_2$-symmetrical dimer generated by C–H···O hydrogen bonds and the formation of the [0 1 0] chain linked by C–H···O hydrogen bonds (dashed lines). For clarity, hydrogens not involved in the motif shown have been omitted. Atoms labeled with an asterisk (*) or an ampersand (&) or a hash (#) sign are at the symmetry positions $(1-x, y, 1/2-z)$, $(x, 1+y, z)$, and $(x, -1+y, z)$, respectively.
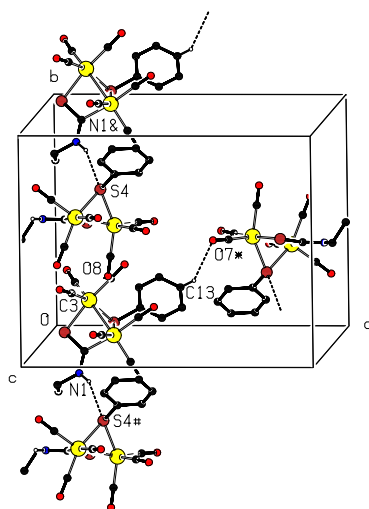
Figure 9. Part of the crystal structure of **4** showing the formation of dimers generated by C–H···O hydrogen bonds and the formation of the [0 1 0] chain linked by N–H···S hydrogen bonds (dashed lines). For clarity, hydrogens not involved in the motif shown have been omitted. Atoms labeled with an asterisk (*) or an ampersand (&) or a hash (#) sign are at the symmetry positions $(1 - x, 1 - y, 1 - z)$, $(x, 1 + y, z)$, and $(x, -1 + y, z)$, respectively.

The dimers (figure 8) are combined into [0 1 0] chains by C8–H8B···O6^{ii} hydrogen bonds [symmetry code: (ii) $x, 1 + y, z$]. Molecules of **4** form dimers via the C13–H13···O7^{i} hydrogen bond [symmetry code: (i) $1 - x, 1 - y, 1 - z$]. The dimers (figure 9) are combined into [0 1 0] chains by the N1–H1N···S4^{ii} hydrogen bond [symmetry code: (ii) $x, -1 + y, z$]. In **5**, molecules generate dimers via the N1–H1N···O5^{i} hydrogen bond [symmetry code: (i) $1 - x, 1 - y, 1 - z$]. The dimers (figure 10) are linked into [1 0 0] chains by the C10–H10A···O1^{ii} hydrogen bond [symmetry code: (ii) $-x, 2 - y, 2 - z$].

3.3. *Spectroscopies of complexes*

The above complexes have been characterized by IR, ^{1}H NMR, and ^{13}C NMR spectroscopies. In IR spectra, the terminal carbonyl groups show three absorptions from 1922 to 2068 cm^{-1}. The NH group occurs at 3304 for **1**, 3089 for **2**, 3367 for **3**, 3390 for **4**, and 3382 cm^{-1} for **5**. Additionally, the MeO$_2$C group appears at 1720 for **1**, 1734 for **2**, and 1728 cm^{-1} for **3**. In ^{1}H NMR spectra, the NH group shows one singlet at 11.454 for **1**, 11.163 for **2**, 7.242 (in DCCl$_3$) for **3**, 7.289 (in DCCl$_3$) for **4**, and 7.164 (in DCCl$_3$) ppm for **5**. As indicated in table 3, low-field NH signals of **1** and **2** are caused by strong intermolecular hydrogen bonds of N–H···O (methoxycarbonyl) for **1** and N–H···N (3-pyridyl) for **2**. The MeO$_2$CCH$_2$ group of **1** as two singlets appears at 3.636 and 2.829 ppm. Unlike **1**, the MeO$_2$CCH$_2$ group in **2** exhibits one singlet at 3.805 ppm and one typical AB quartet due to coupling between the two magnetically nonequivalent protons of the CH$_2$ group, with a ^2J of 13.6 Hz [19, 22(a), 23]. The pyridyl group shows one multiplet for **1**, and two doublets and one singlet for **2**. In **3**, two CH$_3$ groups as two singlets appear at 3.830 (OCH$_3$) and 1.233 ppm whereas two CH$_2$ groups are a multiplet at 3.283–3.415 ppm. As mentioned above, because the signal of the NH group is overlapped with DCCl$_3$, the
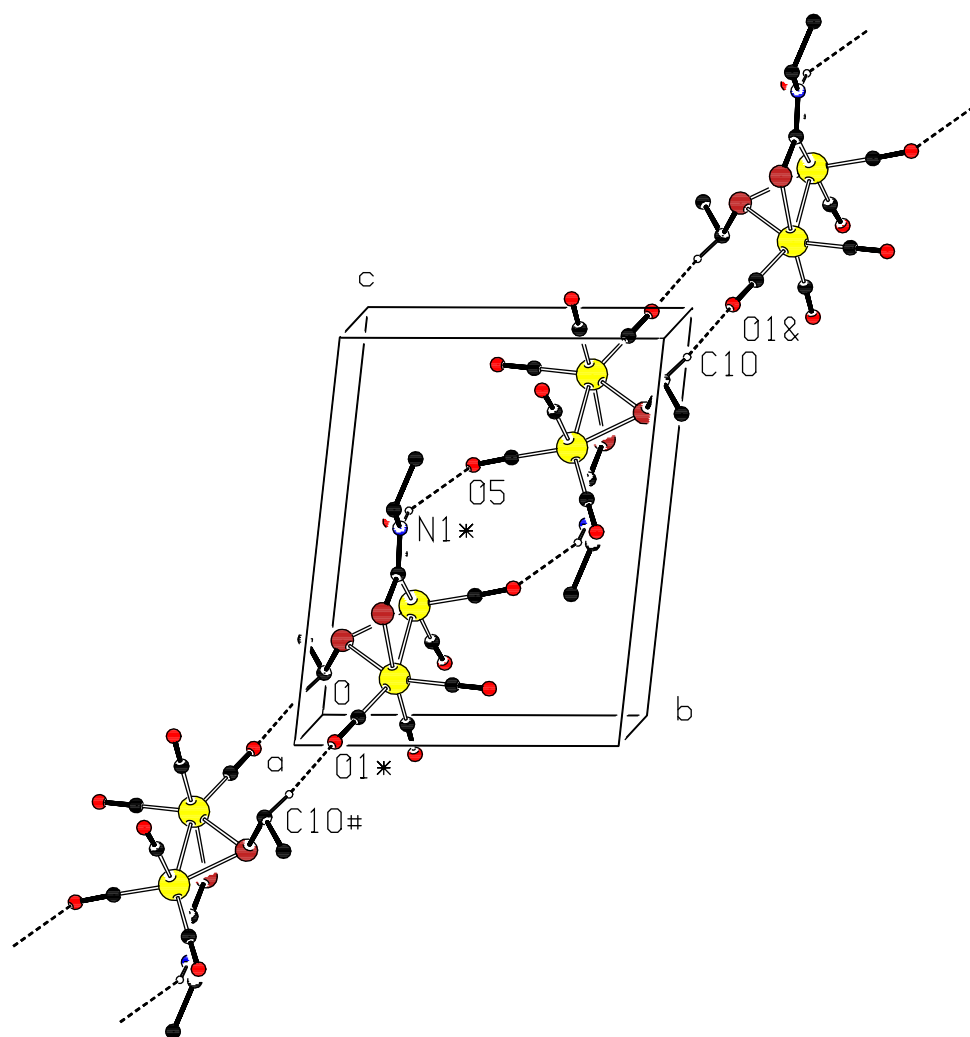
Figure 10.   Part of the crystal structure of **5** showing the formation of dimers generated by N–H⋯O hydrogen bonds and the formation of the [1 1 1] chain linked by C–H⋯O hydrogen bonds (dashed lines). For clarity, hydrogens not involved in the motif shown have been omitted. Atoms labeled with an asterisk (*) or an ampersand (&) or a hash (#) sign are at the symmetry positions $(1-x, 1-y, 1-z)$, $(x, 2-y, 2-z)$, and $(1+x, -1+y, -1+z)$, respectively.

^{1}H NMR spectrum of **3** in acetone-d_6 is also recorded (see Supplementary data). The NH group appears at 9.460 ppm, which is confirmed by D_2O exchange. Therefore, for **3**, the solvent effect of the NH signal owing to the intermolecular N–H⋯O (acetone-d_6) hydrogen bond is observed. The MeO_2CCH_2 group shows one singlet at 3.785 ppm and one typical AB quartet with a ^2J of 13.6 Hz; the NCH_2CH_3 group displays one quartet and triplet with a ^3J of 7.2 Hz. For **4** and **5**, the NCH_2CH_3 group shows one multiplet rather than the expected quartet for CH_2 and triplet for CH_3. Similarly, the CH_3CH_2S group of **5** exhibits the same multiplet. In the ^{13}C NMR spectrum of **1**, the terminal CO groups are four

singlets at 214.003–213.061 ppm, those of **2**, **3**, **4**, and **5** show three singlets from 213.316–207.618, 212.957–208.234, 212.972–208.132, and 213.209–209.122 ppm, indicating their fluxionality on the NMR time scale [18]. The CS group displays one singlet at 160.803 for **1**, 254.014 for **2**, 247.072 for **3**, 247.281 for **4**, and 247.996 ppm for **5**. The high-field shift of the CS group of **1** is in agreement with an sp^3-hybridization [19]. The MeO_2CCH_2 group is three singlets at 51.974 (CH_3), 169.930 ($O=C$), and 40.778 (CH_2) ppm for **1**, at 52.016 (CH_3), 169.561 ($O=C$), and 41.781 (CH_2) ppm for **2**, and at 52.613 (CH_3), 169.714 ($O=C$), and 41.704 (CH_2) ppm for **3**. For **3**, **4**, and **5**, the NCH_2CH_3 group shows one singlet at 44.030, 43.747, and 43.875 ppm for CH_2 and one singlet at 13.341, 12.996, and 13.373 ppm for CH_3. The CH_3CH_2S of **5** exhibits two singlets at 35.398 and 18.538 ppm. As expected, the Ph group of **5** has four peaks. However, the pyridyl groups of **1** and **2** each display four resonances.

3.4. *Electrochemistry of 2 and 5*

In order to evaluate the capability of the above diiron complexes to catalyze hydrogen production, cyclic voltammetry of **2** and **5** has been performed. In MeCN, CV of **2** shows one irreversible oxidation wave at 1.00 V and two irreversible reduction waves at −1.44 and −1.90 V (figure 11). For each step, the peak current varies as the square root of the scan rate in the measured range, consistent with a fast diffusion limited electron transfer (figure 1S).

In CH_2Cl_2, CV of **5** displays one irreversible oxidation at 0.76 V and one irreversible reduction wave at −1.87 V (figures 12, and 2S). In MeCN, CV of **5** exhibits two irreversible oxidation waves at 0.63 and 0.89 V and one irreversible reduction wave at −1.58 V. For each step, the peak current varies as the square root of the scan rate in the measured range, which is in accord with a fast diffusion limited electron transfer (figure 3S).

Because of the p–π conjugation, the N in the SCNH cannot be protonated [38–40]. Therefore, for **2**, the reduction processes may be designated as **2** to **2**$^{1-}$ and **2**$^{1-}$ to **2**$^{2-}$. The
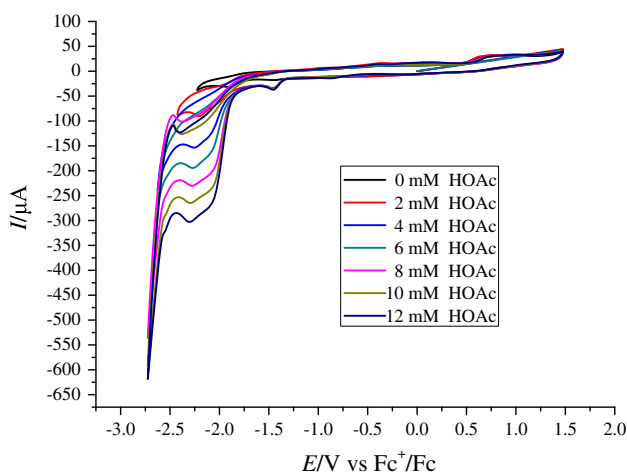

Figure 11.   Cyclic voltammograms of **2** (1.0 mM) with HOAc (0–12 mM) in 0.1 M ^{n}Bu$_4$NPF$_6$/MeCN at a scan rate of 100 mV s^{-1}.
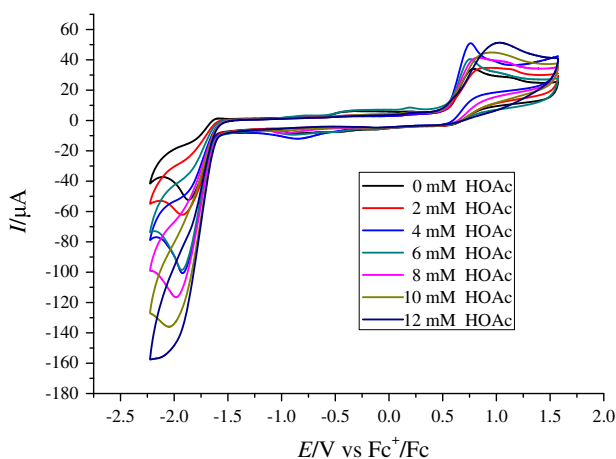
Figure 12. Cyclic voltammograms of **5** (1.0 mM) with HOAc (0–12 mM) in 0.1 M $^{n}Bu_4NPF_6/CH_2Cl_2$ at a scan rate of 100 mV s^{-1}.

oxidation process may be assigned as **2** to **2**$^{1+}$ [6, 38]. As could be seen from figure 11, using HOAc (p$K_a \approx$ 22.3, in CH$_3$CN; $E°$ (vs Fc$^+$/Fc), −1.46 V) as a proton source [41–43], the second reduction peak of **2** exhibits catalytic behavior with an overpotential of −0.44 V; the reduction current increases and the position of this peak shifts to a more negative potential with increasing concentration of acetic acid added [44–47]; the formed H$_2$ was confirmed by GC. For **5**, the reduction process may be designated as **5** to **5**$^{1-}$. The oxidation process in CH$_2$Cl$_2$ may be assigned as **5** to **5**$^{1+}$ [6, 38]. As shown in figure 12, the reduction peak of **5** shows catalytic behavior; with increasing amount of acetic acid, the reduction current increases [44–47]. According to a criterion of CE (catalytic efficiency = $(i_{cat}/i_d)/(C_{HA}/C_{cat})$, where i_{cat} is the catalytic current, i_d is the current for reduction of the catalyst in the absence of acid, C_{HA} is the acid concentration, and C_{cat} is the catalyst concentration) proposed by Lichtenberger *et al.*, CE is 0.99 and 0.62 for **2** and **5** (0.36 in MeCN), respectively [6].

4. Conclusion

Reactions of the [Et$_3$NH][(μ-RS)Fe$_2$(CO)$_6$(μ-CO)] with isothiocyanates have been investigated. The reaction of MeO$_2$CCH$_2$SH, Et$_3$N, and Fe$_3$(CO)$_{12}$ with 2-C$_5$H$_4$NNCS forms **1**, (μ-MeO$_2$CCH$_2$S)Fe$_2$(CO)$_5$(μ-k^{2}N,S:k^{2}C-2-C$_5$H$_4$NNHCS); the reactions with 3-C$_5$H$_4$NNCS and EtNCS provide **2**, (μ-MeO$_2$CCH$_2$S)Fe$_2$(CO)$_6$(μ-k^{2}C,S-3-C$_5$H$_4$NNHCS) and **3**, (μ-MeO$_2$CCH$_2$S)Fe$_2$(CO)$_6$(μ-k^{2}C,S-EtNHCS). The reaction of PhSH, Et$_3$N, and Fe$_3$(CO)$_{12}$ with EtNCS affords **4**, (μ-PhS)Fe$_2$(CO)$_6$(μ-k^{2}C,S-EtNHCS). The reaction of EtSH, Et$_3$N, and Fe$_3$(CO)$_{12}$ with EtNCS gives **5**, (μ-EtS)Fe$_2$(CO)$_6$(μ-k^{2}C,S-EtNHCS). Their structures have been unambiguously determined by X-ray crystallography. Electrochemical studies on **2** and **5** confirm that **2** shows high H$_2$-producing activity.

Supplementary material

CCDC 1007551 (**1**), 1041326 (**1**), 1041327 (**2**), 1043327 (**3**), 1007552 (**4**), and 1007553 (**5**) contain the supplementary crystallographic data (including structure factors) for this article. These data can be obtained free of charge from the Cambridge Crystallographic Data Center via www.ccdc.cam.ac.uk/data_request/cif.

Acknowledgements

Disclosure statement

The authors declare no competing financial interest.

Supplemental data

Supplemental data for this article can be accessed here [http://dx.doi.org/10.1080/00958972.2015.1048689].

References

[1] (a) T.R. Simmons, G. Berggren, M. Bacchi, M. Fontecave, V. Artero. *Coord. Chem. Rev.*, **270–271**, 127 (2014); (b) W. Lubitz, H. Ogata, O. Rüdiger, E. Reijerse. *Chem. Rev.*, **114**, 4081 (2014).
[2] J.-F. Capon, F. Gloaguen, F.Y. Pétillon, P. Schollhammer, J. Talarmin. *Coord. Chem. Rev.*, **253**, 1476 (2009).
[3] C. Tard, C.J. Pickett. *Chem. Rev.*, **109**, 2245 (2009).
[4] F. Gloaguen, T.B. Rauchfuss. *Chem. Soc. Rev.*, **38**, 100 (2009).
[5] D.M. Heinekey. *J. Organomet. Chem.*, **694**, 2671 (2009).
[6] G.A.N. Felton, C.A. Mebi, B.J. Petro, A.K. Vannucci, D.H. Evans, R.S. Glass, D.L. Lichtenberger. *J. Organomet. Chem.*, **694**, 2681 (2009).
[7] A.D. Wilson, R.K. Shoemaker, A. Miedaner, J.T. Muckerman, D.L. DuBois, M.R. DuBois. *Proc. Nat. Acad. Sci. USA*, **104**, 6951 (2007).
[8] L.-C. Song, M.-Y. Tang, F.-H. Su, Q.-M. Hu. *Angew. Chem. Int. Ed.*, **45**, 1130 (2006).
[9] M.L. Singleton, N. Bhuvanesh, J.H. Reibenspies, M.Y. Darensbourg. *Angew. Chem. Int. Ed.*, **47**, 9492 (2008).
[10] Ö.F. Erdem, L. Schwartz, M. Stein, A. Silakov, S. Kaur-Ghumaan, P. Huang, S. Ott, E.J. Reijerse, W. Lubitz. *Angew. Chem. Int. Ed.*, **50**, 1439 (2011).
[11] Y.-C. Liu, K.-T. Chu, R.-L. Jhang, G.-H. Lee, M.-H. Chiang. *Chem. Commun.*, **49**, 4743 (2013).
[12] M.R. DuBois, D.L. DuBois. *Chem. Soc. Rev.*, **38**, 62 (2009).
[13] A. Le Goff, V. Artero, B. Jousselme, P.D. Tran, N. Guillet, R. Métayé, A. Fihri, S. Palacin, M. Fontecave. *Science*, **326**, 1384 (2009).
[14] S.C. Marinescu, J.R. Winkler, H.B. Gray. *Proc. Nat. Acad. Sci. USA*, **109**, 15127 (2012).
[15] Y.-C. Shi, H. Tan, Y. Shi. *Polyhedron*, **67**, 218 (2014).
[16] Y.-C. Shi, W. Yang, Y. Shi, D.-C. Cheng. *J. Coord. Chem.*, **67**, 2330 (2014).
[17] W. Yang, Q. Fu, J. Zhao, H.-R. Cheng, Y.-C. Shi. *Acta Crystallogr.*, **C70**, 528 (2014).
[18] Y.-C. Shi, F. Gu. *Chem. Commun.*, **49**, 2255 (2013).
[19] Y.-C. Shi, H.-R. Cheng, Q. Fu, F. Gu, Y.-H. Wu. *Polyhedron*, **56**, 160 (2013).
[20] Y.-C. Shi, Q. Fu. *Z. Anorg. Allg. Chem.*, **639**, 1791 (2013).
[21] Y.-C. Shi, H.-R. Cheng, D.-C. Cheng. *Acta Crystallogr.*, **C69**, 581 (2013).

[22] (a) Y.-C. Shi, H.-R. Cheng, H. Tan. *J. Organomet. Chem.*, **716**, 39 (2012); (b) Y.-C. Shi, H.-R. Cheng, L.-M. Yuan, Q.-K. Li. *Acta Crystallogr.*, **E67**, m1534 (2011).
[23] Y.-C. Shi, Y. Shi, W. Yang. *J. Organomet. Chem.*, **772–773**, 131 (2014).
[24] G. L'abbé. *Synthesis*, **1987**, 525 (1987).
[25] M.C. Burla, R. Caliandro, M. Camalli, B. Carrozzini, G.L. Cascarano, C. Giacovazzo, M. Mallamo, A. Mazzone, G. Polidori, R. Spagna. *J. Appl. Crystallogr.*, **45**, 357 (2012).
[26] G.M. Sheldrick. *Acta Crystallogr.,* **A64**, 112 (2008).
[27] A.L. Spek. *Acta Crystallogr.,* **D65**, 148 (2009).
[28] L.-C. Song. *Acc. Chem. Res.*, **38**, 21 (2005).
[29] L.-C. Song. *Sci. China Ser. B-Chem.*, **52**, 1 (2009).
[30] D. Seyferth, G.B. Womack, C.M. Archer, J.C. Dewan. *Organometallics*, **8**, 430 (1989).
[31] D. Seyferth, G.B. Womack, C.M. Archer, J.P. Fackler, D.O. Marler. *Organometallics*, **8**, 443 (1989).
[32] L.-C. Song, Q.-M. Hu, H.-T. Fan, B.-W. Sun, M.-Y. Tang, Y. Chen, Y. Sun, C.-X. Sun, Q.-J. Wu. *Organometallics*, **19**, 3909 (2000).
[33] L.-C. Song, G.-L. Lu, Q.-M. Hu, H.-T. Fan, J.-B. Chen, J. Sun, X.-Y. Huang. *J. Organomet. Chem.*, **627**, 255 (2001).
[34] K.-H. Yih, H.-F. Wang, G.-H. Lee. *Acta Crystallogr.*, **E66**, m1189 (2010).
[35] H.-F. Wang, K.-H. Yih, G.-H. Lee, S.-L. Huang. *J. Chin. Chem. Soc.*, **58**, 15 (2011).
[36] K.-H. Yih, H.-F. Wang, G.-H. Lee, S.-L. Huang. *J. Chin. Chem. Soc.*, **58**, 262 (2011).
[37] D. Berger, M. Erdmann, J. Notni, W. Imhof. *CrystEngComm*, **2**, 24 (2000).
[38] (a) Z. Wang, W.-F. Jiang, J.-H. Liu, W.-N. Jiang, Y. Wang, B. Åkermark, L.-C. Sun. *J. Organomet. Chem.*, **693**, 2828 (2008); (b) M. Karnahl, A. Orthaber, S. Tschierlei, L. Nagarajan, S. Ott. *J. Coord. Chem.*, **65**, 2713 (2012).
[39] S. Ezzaher, J.-F. Capon, F. Gloaguen, F.Y. Pétillon, P. Schollhammer, J. Talarmin. *Inorg. Chem.*, **48**, 2 (2009).
[40] M.R. DuBois, D.L. DuBois. *C. R. Chimie*, **11**, 805 (2008).
[41] G.A.N. Felton, A.K. Vannucci, N. Okumura, L.T. Lockett, D.H. Evans, R.S. Glass, D.L. Lichtenberger. *Organometallics*, **27**, 4671 (2008).
[42] J.-F. Capon, F. Gloaguen, P. Schollhammer, J. Talarmin. *J. Electroanal. Chem.*, **595**, 47 (2006).
[43] G.A.N. Felton, R.S. Glass, D.L. Lichtenberger, D.H. Evans. *Inorg. Chem.*, **45**, 9181 (2006).
[44] I. Bhugun, D. Lexa, J.-M. Savéant. *J. Am. Chem. Soc.*, **118**, 3982 (1996).
[45] F. Gloaguen, J.D. Lawrence, T.B. Rauchfuss. *J. Am. Chem. Soc.*, **123**, 9476 (2001).
[46] L.-C. Song, C.-G. Li, J. Gao, B.-S. Yin, X. Luo, X.-G. Zhang, H.-L. Bao, Q.-M. Hu. *Inorg. Chem.*, **47**, 4545 (2008).
[47] G. Durgaprasad, R. Bolligarla, S.K. Das. *J. Organomet. Chem.*, **696**, 3097 (2011).